Journal of Molecular Structure 1120 (2016) 317–326

Contents lists available at ScienceDirect

Journal of Molecular Structure

journal homepage: http://www.elsevier.com/locate/molstruc

Spectroscopic investigations and molecular docking study of (2*E*)-1-(4-Chlorophenyl)-3-[4-(propan-2-yl)phenyl]prop-2-en-1-one using quantum chemical calculations

Shana Parveen [a], Monirah A. Al-Alshaikh [b], C. Yohannan Panicker [c, *], Ali A. El-Emam [d], Vinutha V. Salian [e], B. Narayana [e], B.K. Sarojini [f], C. van Alsenoy [g]

[a] Department of Physics, TKM College of Arts and Science, Kollam, Kerala, India
[b] Department of Chemistry, College of Sciences, King Saud University, Riyadh 11451, Saudi Arabia
[c] Department of Physics, Fatima Mata National College, Kollam, Kerala, India
[d] Department of Pharmaceutical Chemistry, College of Pharmacy, King Saud University, Riyadh 11451, Saudi Arabia
[e] Department of Studies in Chemistry, Mangalore University, Mangalagangotri, Karnataka, India
[f] Department of Studies in Industrial Chemistry, Mangalore University, Mangalagangothri, Karanataka, India
[g] Department of Chemistry, University of Antwerp, Groenenborgerlaan 171, Antwerp B-2020, Belgium

ARTICLE INFO

Article history:
Received 27 October 2015
Received in revised form
10 March 2016
Accepted 10 May 2016
Available online 12 May 2016

Keywords:
DFT
FT-IR
FT-Raman
Hyperpolrizability
Molecular docking

ABSTRACT

In this work, the vibrational spectral analysis was carried out using FT-IR and FT-Raman spectroscopy of (2*E*)-1-(4-Chlorophenyl)-3-[4-(propan-2-yl)phenyl]prop-2-en-1-one. The computations were performed at DFT level of theory to get the optimizedgeometry and vibrational wave numbers of the normal modes of the title compound using Gaussian09 software. The complete vibrational assignments of wave numbers were made on the basis of potential energy distribution. The calculated HOMO and LUMO energies show chemical activity of the molecule. The stability of the molecule arising from hyperconjugative interaction and charge delocalization has been analyzed using NBO analysis. The hyperpolarizability values are reported and the first hyperpolarizability of the title compound is 83.85 times that of standard NLO material urea. From the MEP plot, the negative electrostatic potential regions are mainly localized over the carbonyl group, the phenyl rings and are possible sites for electrophilic attack. The positive regions are localized over all the hydrogen atoms and are possible sites for nucleophilic attack. The molecular docking results suggest that the compound might exhibit inhibitory activity against lymphocyte-specific kinase and may results in design of novel T-cell immunosuppressants.

1. Introduction

Chalcones are an important class of natural compounds and have been widely applied as synthons in synthetic organic chemistry. The nonlinear optical properties of the different chalcone derivatives have been reported [1–4]. These, α,β-unsaturated ketones possess a wide variety of biological activities, including antileishmanial [5], anticancer [6,7], anti-invasive [8], anti-tuberculosis [9], antimicrobial [10,11], anti-malarial [12], antitumor [13,14], antiproliferative [15] and anti-oxidant activity [16]. Asiri et al. [17] reported the synthesis, molecular structure, spectral investigation on (E)-1-(4-bromophenyl)-3-(4-(dimethylamino)phenyl)prop-2-en-one. Parveen et al. [18] reported the vibrational and structural observations and molecular docking study on 1-{3-(4-chlorophenyl)-5-[4-(propan-2-yl)phenyl]-4,5-dihydro-1H-pyrazol-1-yl}-ethanone. The synthesis and molecular structure of 2-bromo-N-(7-(diethylamino)-coumarin-3-yl)phenyl)propanamide is reported by Kulai and Mallet-Ladeira [19]. Solid state stuctural and theoretical investigations of a biologically active chalcone is reported in literature [20]. Demir et al. [21] reported the vibrational spectroscopic studies of 1-(2-nitrobenzoyl)-3,5-diphenyl-4,5-dihydro-1H-pyrazole with X-ray diffractions and DFT calculations. The crystal structures of some chalcone derivatives *viz*., a second polymorph of (2*E*)-1-(4-fluorophenyl)-3-(3,4,5-trimethoxyphenyl)prop-2-en-1-one, 2,3-dibromo-1,3-bis(4-fluorophenyl)propan-1-one, (2*E*)-1-(3,4-dichlorophenyl)-3-(2-hydroxyphenyl) prop-2-en-1-one [22–24], 3-(3,4-dimethoxyphenyl)-1-(4-fluorophenyl) prop-2-en-

* Corresponding author.
E-mail address: cyphyp@rediffmail.com (C.Y. Panicker).

http://dx.doi.org/10.1016/j.molstruc.2016.05.030
0022-2860/

1-one, 2,3-dibromo-1-(4-ethoxyphenyl)-3-[4-(methylsulfanyl) phenyl]propan-1-one, 2-bromo-1-(4-methylphenyl)-3-[4-(methylsulfanyl)phenyl]prop-2-en-1-one, (2E)-1-(2,4-dichloro phenyl)-3-[4-(methylsulfanyl)phenyl]prop-2-en-1-one [25–28] and 2-bromo-1-chlorophenyl-3-(4-methoxyphenyl) prop-2-en-1-one [29] have been reported. Mary et al. [30,31] reported the molecular conformational analysis, vibrational spectra, NBO analysis and first hyperpolarizability of (2E)-3-phenylprop-2-enoic anhydride and (2E)-3-(3-chlorophenyl)prop-2-enoic anhydride based on density functional theory calculations.

Chloro-substituted cinnamic acids have received attention in the field of tumor treatment and the chloro-substituted phenyl analogues, on the other hand, have been proven to perform as efficient as the respective parent cinnamic acid without producing the side effects observed by the parent compounds [32]. In the present work, IR and Raman spectra of the title compound are reported both experimentally and theoretically. Also NBO, HOMO-LUMO, molecular electrostatic potential, first and second hyperpolarizability studies are reported. Due to the different potential biological activity of the title compound, molecular docking study is also reported.

2. Experimental details

The compound was prepared (Scheme 1) following the literature method reported [33]. Re-crystallized from ethanol (M.P.: 343–345 K).

2.1. Reaction scheme

The FT-IR spectrum (Fig. 1) was recorded using KBr pellets on a DR/Jasco FT-IR 6300 spectrometer. The FT-Raman spectrum (Fig. 2) was obtained on a Bruker RFS 100/s, Germany. For excitation of the spectrum the emission of Nd:YAG laser was used, excitation wavelength 1064 nm, maximal power 150 mW, measurement on solid sample. The deconvoluted experimental IR and Raman spectra are provided as Fig.S1 and Fig.S2 (supporting material).

3. Computational details

For meeting the requirements of both accuracy and computing economy, theoretical methods and basis sets should be considered. Density functional theory has been proven to be extremely useful in treating the electronic structure of the molecules. Gaussian09 program [34] was used to carry out DFT calculations with Becke's three-parameter hybrid model and the Lee-Yang-Parr correlation functional (B3LYP) method. The basis set B3LYP/6-31++G(d) (6D, 7F), which is an effective level with a reasonable cost to study fairly large organic molecules, was utilized. As the DFT hybrid B3LYP functional tends to overestimate the frequencies of the fundamental modes; scaling factors have to be used for obtaining a considerably better agreement with experimental data. Thus, a scaling factor of 0.9613 has been uniformly applied to the B3LYP calculated wavenumbers [35]. The assignments of the calculated wave numbers are aided by the animation option of GAUSSVIEW program, which gives a visual presentation of the vibrational modes [36] and the potential energy distribution (PED) values were calculated with the help of GAR2PED software package [37]. The

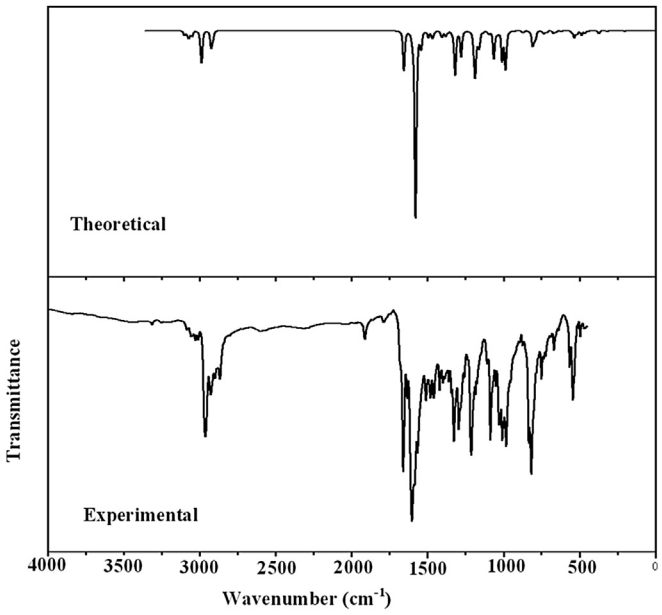

Fig. 1. FT-IR spectrum of (2*E*)-1-(4-chlorophenyl)-3-[4-(propan-2-yl)phenyl]prop-2-en-1-one.

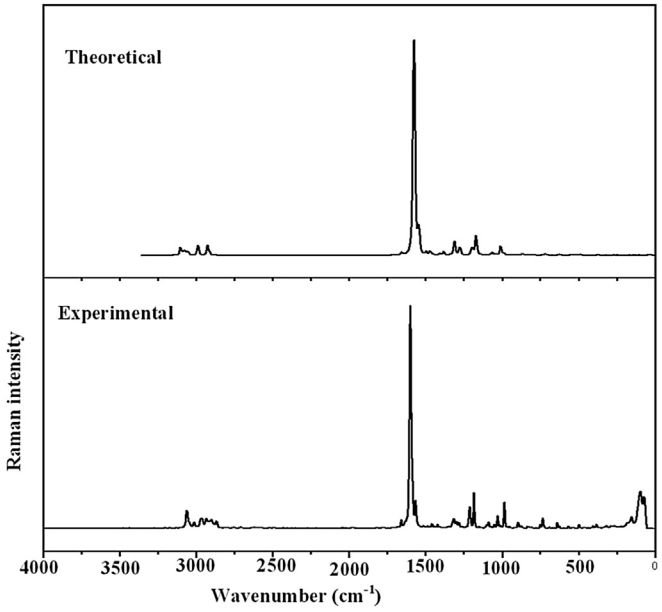

Fig. 2. FT-Raman spectrum of (2*E*)-1-(4-chlorophenyl)-3-[4-(propan-2-yl)phenyl] prop-2-en-1-one.

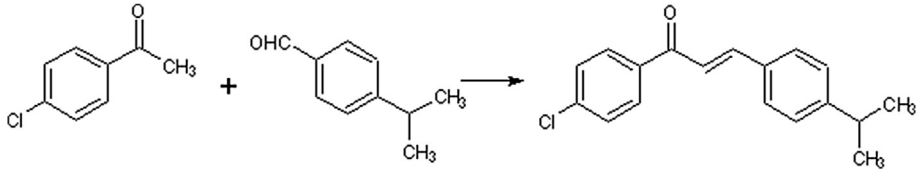

Scheme 1. Scheme-synthesis pathway of the title compound.

optimized geometrical parameters (Fig. 3) with XRD data are given in Table 1.

4. Results and discussion

4.1. IR and Raman spectra

The observed IR and Raman bands and calculated (scaled) wavenumbers and assignments are given in Table 2. The carbonyl stretching C=O vibration [38–40] is expected in the region 1750-1600 cm^{-1} and in the present case the C=O mode appears at 1660 cm^{-1} in the IR spectrum, 1659 cm^{-1} in the Raman spectrum and at 1656 cm^{-1} theoretically. The in-plane and out-of-plane C=O deformations are expected in the regions 625 ± 70 and 540 ± 80 cm^{-1}, respectively [38]. The C=O deformation bands are observed at 669 cm^{-1} in the IR spectrum, 648 cm^{-1} in the Raman spectrum and at 671, 656 cm^{-1} theoretically. Mary et al. [30] reported the C=O modes at 1768, 1701, 804 cm^{-1} in the IR spectrum, 1763, 1697, 779, 697 cm^{-1} in the Raman spectrum and at 1768, 1702, 799, 771, 691, 653 cm^{-1} theoretically.

According to Socrates [41] the C=C stretching is expected around 1600 cm^{-1} when conjugated with C=O group. For the title compound, the bands observed at 1578 cm^{-1} in the IR spectrum and at 1580 cm^{-1} theoretically are assigned as C=C stretching mode. Mary et al. [30] reported the C=C stretching mode at 1620 cm^{-1} in the IR spectrum, 1621, 1601 cm^{-1} in the Raman spectrum and at 1611, 1607 cm^{-1} theoretically.

The methyl stretching modes are expected in the region 2900-3000 cm^{-1} [38]. The bands observed at 2975, 2929 cm^{-1} in the IR spectrum, 2972, 2930 cm^{-1} the Raman spectrum and in the range 2921–2993 cm^{-1} theoretically are assigned as these modes for the title compound. For the title compound, the methyl deformation modes are observed at 1462, 1362 cm^{-1} in the IR spectrum, 1459 cm^{-1} in the Raman spectrum and in the range 1470–1365 cm^{-1} theoretically as expected [38]. The first methyl rocking vibration [38] has been observed at 1190 ± 45 cm^{-1} and the second methyl rock [38] absorb at 950 ± 30 cm^{-1}. These modes calculated (DFT) at 1136, 1040, 931, 904 cm^{-1} were assigned as rocking modes of the methyl group. These modes are observed at 1035, 898 cm^{-1} in the Raman spectrum.

For simple organic chlorine compounds, C–Cl absorptions are in the region 750-700 cm^{-1}. Sundaraganesan et al. [42] reported C–Cl stretching at 704 (IR), 705 (Raman), and 715 cm^{-1} (DFT) and the deformation bands at 250 and 160 cm^{-1}. Renjith et al. [43] reported the C–Cl stretching modes in the range 609–947 cm^{-1}. For the title compound, the band at 706 cm^{-1} (DFT) is assigned as C–Cl stretching modes. The deformation bands of C–Cl are also identified. This is in agreement with the literature data [44]. Mary et al. [45] reported the CCl stretching mode at 671 cm^{-1} theoretically.

In the following discussion, the para substituted phenyl ring with chlorine is designated as PhI and the other para-substituted phenyl ring as PhII. The C–H stretching modes occurs above 3000 cm^{-1} and is typically exhibited as a multiplicity of weak to moderate bands, compared with the aliphatic C–H stretch [46]. For the title compound, CH stretching vibrations of the phenyl rings are assigned in the range 3103–3081 cm^{-1} for PhI and 3075-3052 cm^{-1} for PhII theoretically. The phenyl CH stretching modes are observed at 3083, 3053 cm^{-1} in the IR spectrum and at 3057 cm^{-1} in the Raman spectrum.

The DFT calculations give the phenyl ring stretching modes in the range 1572–1289 cm^{-1} for PhI and in the range 1599–1272 cm^{-1} for PhII as expected [38]. The bands observed at 1603, 1488, 1403, 1382, 1292 cm^{-1} in the IR spectrum and at 1600, 1568, 1525 cm^{-1} in the Raman spectrum are assigned as the phenyl ring stretching modes. The ring breathing mode of the 1,4-disubstituted benzenes with entirely different substituent [47] has been reported in the interval 700-880 cm^{-1}. For the title compound, the ring breathing modes are assigned at 720, 734 cm^{-1} in the IR spectrum, 734 cm^{-1} in the Raman spectrum and at 736, 717 cm^{-1} theoretically.

The in-plane CH deformation bands of the phenyl ring are expected above 1000 cm^{-1} [38] and in the present case, the bands at 1281, 1172, 1155, 1105, 1090, 1059 cm^{-1} (IR), 1282, 1092, 1058 cm^{-1} in Raman spectrum and in the range 1276–1064 cm^{-1} for PhI and 994-1279 cm^{-1} for PhII (DFT) are assigned as the in-plane CH deformation modes.

The CH out-of-plane deformations of the phenyl ring [38] are observed between 1000 and 700 cm^{-1}. The bands observed at 954, 830, 812 cm^{-1} in IR spectrum and in the range 957–801 (DFT) for PhI and 943-811 cm^{-1} (DFT) are assigned as the CH out-of-plane deformations of the phenyl rings. Most of the modes are not pure but contains a significant contribution from other modes also. In order to investigate the performance of vibrational wavenumbers of the title compound, the root mean square value between the calculated and observed wavenumbers were calculated and the RMS errors are 3.76 for IR and 4.98 for Raman modes.

4.2. Geometrical parameters

The aromatic ring of the title compound is somewhat irregular and the spread of C–C bond distance is (DFT/XRD) 1.3918–1.4053/1.3596–1.4026 Å in PhI and 1.3917–1.4091/1.3606–1.4015 Å in PhII, which is similar to the spread reported by Bhagyasree et al. [48]. For the title compound, the C=O and C=C bond lengths (DFT/XRD) are 1.2323/1.2275 Å and 1.3518/1.3207 Å, respectively. For the title compound, the CCl bond length (DFT/XRD) is 1.7558/1.7435 Å,

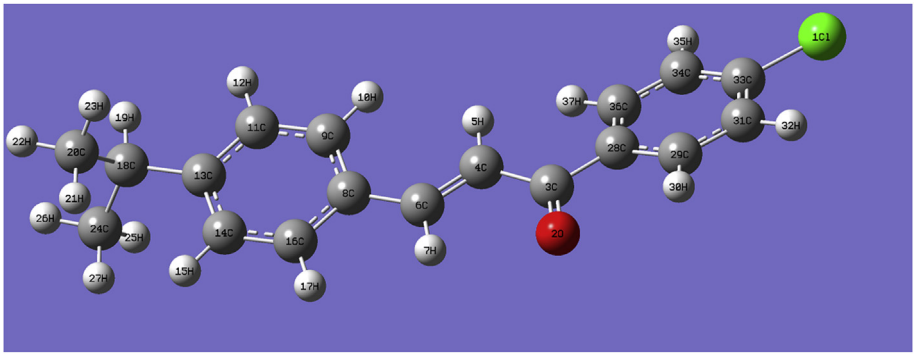

Fig. 3. Optimized geometry of (2*E*)-1-(4-chlorophenyl)-3-[4-(propan-2-yl)phenyl]prop-2-en-1-one.

Table 1
Optimized geometrical parameters of (2*E*)-1-(4-Chlorophenyl)-3-[4-(propan-2-yl) phenyl]prop-2-en-1-one.

Bond lengths (Å) (DFT/XRD)			
C33–Cl1	1.7558/1.7435	C3–O2	1.2323/1.2275
C3–C4	1.4810/1.4855	C3–C28	1.5037/1.4746
C4–H5	1.0850/0.9500	C4–C6	1.3518/1.3207
C6–H7	1.0896/0.9500	C6–C8	1.4610/1.4696
C8–C9	1.4086/1.3966	C8–C16	1.4091/1.3656
C9–H10	1.0865/0.9500	C9–C11	1.3917/1.3756
C11–H12	1.0882/0.9500	C11–C13	1.4054/1.3826
C13–C14	1.4038/1.4015	C13–C18	1.5219/1.5105
C14–H15	1.0874/0.9500	C14–C16	1.3927/1.3606
C16–H17	1.0878/0.9500	C18–H19	1.0988/1.0000
C18–C20	1.5419/1.5256	C18–C24	1.5417/1.5357
C20–H21	1.0969/0.9800	C20–H22	1.0969/0.9800
C20–H23	1.0959/0.9800	C24–H25	1.0959/0.9800
C24–H26	1.0969/0.9800	C24–H27	1.0968/0.9800
C28–C29	1.4053/1.3955	C28–C36	1.4042/1.4026
C29–H30	1.0854/0.9500	C29–C31	1.3918/1.3686
C31–H32	1.0853/0.9500	C31–C33	1.3976/1.3866
C33–C34	1.3949/1.3596	C34–H35	1.0852/0.9500
C34–C36	1.3958/1.3787	C36–H37	1.0851/0.9500
Bond angles (°) (DFT/XRD)			
O2–C3–C4	121.6/122.0	O2–C3–C28	119.5/121.0
C4–C3–C28	119.0/116.9	C3–C4–H5	118.5/119.9
C3–C4–C6	120.5/120.2	H5–C4–C6	120.9/119.9
C4–C6–H7	116.2/116.4	C4–C6–C8	128.0/127.3
H7–C6–C8	115.8/116.4	C6–C8–C9	123.7/121.8
C6–C8–C16	118.8/119.7	C9–C8–C16	117.5/118.5
C8–C9–H10	120.1/119.9	C8–C9–C11	120.9/120.3
H10–C9–C11	119.1/119.9	C9–C11–H12	119.2/119.4
C9–C11–C13	121.6/121.2	H12–C11–C13	119.2/119.4
C11–C13–C14	117.6/117.6	C11–C13–C18	120.7/121.2
C14–C13–C18	121.7/121.2	C13–C14–H15	120.0/119.6
C13–C14–C16	121.1/120.8	H15–C14–C16	119.0/119.6
C8–C16–C14	121.4/121.6	C8–C16–H17	119.0/119.2
C14–C16–H17	119.6/119.2	C13–C18–H19	107.0/107.9
C13–C18–C20	111.9/112.1	C13–C18–C24	111.8/110.4
H19–C18–C20	107.4/107.9	H19–C18–C24	107.4/107.9
C20–C18–C24	111.0/110.4	C18–C20–H21	111.3/109.5
C18–C20–H22	110.4/109.5	C18–C20–C23	111.3/110.1
H21–C20–H22	107.7/109.5	H21–C20–H23	107.8/109.5
H22–C20–H23	108.2/109.5	C18–C24–H25	111.3/109.5
C18–C24–H26	110.4/109.5	C18–C24–H27	111.3/109.5
H25–C24–H26	108.2/109.5	H25–C24–H27	107.8/109.5
H26–C24–H27	107.7/109.5	C3–C28–C29	117.9/120.4
C3–C28–C36	123.6/122.6	C29–C28–C36	118.5/117.0
C28–C29–H30	118.4/119.4	C28–C29–C31	121.2/121.2
H30–C29–C31	120.4/119.4	C29–C31–H32	120.8/120.2
C29–C31–C33	119.1/119.6	H32–C31–C33	120.1/120.2
Cl1–C33–C31	119.5/119.9	Cl1–C33–C34	119.4/118.6
C31–C33–C34	121.1/121.5	C33–C34–H35	120.2/120.7
C33–C34–C36	119.1/118.5	H35–C34–C36	120.7/120.7
C28–C36–C34	121.0/122.2	C28–C36–H37	120.8/118.9
C34–C36–H37	118.2/118.9		
Dihedral angles (°) (DFT/XRD)			
O2–C3–C4–C6	−6.4/-13.2	C28–C3–C4–C6	174.4/162.3
O2–C3–C28–C29	−14.1/-25.1	O2–C3–C28–C36	164.4/152.1
C4–C3–C28–C29	165.1/159.6	C4–C3–C28–C36	−16.4/-23.5
C3–C4–C6–C8	179.1/176.1	C4–C6–C8–C9	−2.8/-16.9
C4–C6–C8–C16	177.3/165.7	C6–C8–C9–C11	179.9/178.8
C16–C8–C9–C11	−0.2/-1.3	C6–C8–C16–C14	−179.9/-179.9
C9–C8–C16–C14	0.2/2.1	C8–C9–C11–C13	−0.0/0.2
C9–C11–C13–C14	0.2/0.1	C9–C11–C13–C18	−179.9/-179.8
C11–C13–C14–C16	−0.1/.9	C18–C13–C14–C16	179.9/179.3
C11–C13–C18–C20	−117.0/-115.4	C11–C13–C18–C24	117.7/121.0
C14–C13–C18–C20	62.9/64.3	C14–C13–C18–C24	−62.3/-59.3
C13–C14–C16–C8	−0.1/-2.2	C3–C28–C29–C31	179.3/
C36–C28–C29–C31	0.7/0.6	C3–C28–C36–C34	−178.6/-175.9
C29–C28–C36–C34	−0.1/1.2	C28–C29–C31–C33	−0.7/-1.7
C29–C31–C33–Cl1	−179.8/-179.3	C29–C31–C33–C34	0.0/1.2
Cl1–C33–C34–C36	−179.5/-179.1	C31–C33–C34–C36	0.6/0.6
C33–C34–C36–C28	−0.6/-1.7		

while Mary et al. [49] reported the CCl bond length as 1.7581 Å (DFT).

The bond lengths of the title compound (DFT/XRD), C_6–C_8 = 1.4610/1.4696, C_4–C_3 = 1.4810/1.4855, C_3–C_{28} = 1.5033/1.4746, C_{13}–C_{18} = 1.5219/1.5105, C_{18}–C_{20} = 1.5419/1.5256 and C_{18}–C_{24} = 1.5417/1.5357 Å which clearly shows the typical single bond character and the elongation is due to the presence of adjacent groups as reported in literature [49].

At C_{28} position, the bond angles, C_{36}–C_{28}–C_3 is increased by 3.6° and C_{29}–C_{28}–C_3 is reduced by 2.1°, from 120°, which reveals the interaction between carbonyl group and H_{30}. At C_3 position, the bond angles (DFT/XRD) are C_4–C_3–C_{28} = 119.0/116.9, C_4–C_3–O_2 = 121.6/122.0 and C_{28}–C_3–O_2 = 119.5/121.0° and this asymmetry in bond angles reveal the interaction between C=O and C=C bonds. Similarly at C_8 position, the bond angles (DFT/XRD) C_9–C_8–C_{16} = 117.5/118.5, C_9–C_8–C_6 = 123.7/121.8 and C_{16}–C_8–C_6 = 118.8/119.7° and this asymmetry is due to the presence of the adjacent C=C group.

Due to the high electronegativity of chlorine atom, the bond angle (DFT/XRD) C_{31}–C_{33}–C_{34} increased by 1.1/1.5°, from 120° as reported in literature [49]. The methyl groups are tilted from the phenyl ring PhII, as is evident from the torsion angles (DFT/XRD) C_9–C_{11}–C_{13}–C_{18} = −179.9/-179.9, C_{11}–C_{13}–C_{18}–C_{20} = −117.0/-115.4, C_{11}–C_{13}–C_{18}–C_{24} = 117.7/121.0, C_{16}–C_{14}–C_{13}–C_{18} = 179.9/179.3, C_{14}–C_{13}–C_{18}–C_{20} = 62.9/64.3 and C_{14}–C_{13}–C_{18}–C_{24} = −62.3/-59.3°. Also the carbonyl group is tilted from the phenyl ring PhI which is evident from the torsion angles (DFT/XRD) C_{34}–C_{36}–C_{28}–C_3 = −178.6/-175.0, C_{36}–C_{28}–C_3–C_4 = −16.4/-23.5, C_{31}–C_{29}–C_{28}–C_3 = 179.3/177.7 and C_{29}–C_{28}–C_3–C_4 = 165.1/159.6°.

4.3. Frontier molecular orbitals

Knowledge of the highest occupied molecular orbital (HOMO) and lowest unoccupied molecular orbital (LUMO) and their properties such as their energy is very useful to gauge the chemical reactivity of the molecule. The ability of the molecule to donate an electron is associated with the HOMO and the characteristic of the LUMO is associated with the molecule's electron affinity. The HOMO and LUMO energies are very useful for physicists and chemists and are very important terms in quantum chemistry [50]. The pictorial representation of the HOMO and the LUMO is shown in Fig. 4. The HOMO lies at −8.181 eV and whereas the LUMO is located at −6.061 eV and HOMO is delocalized over the phenyl ring PhI and the carbonyl group while LUMO is delocalized over the entire molecule. This shows that an eventual charge transfer occurs within the molecule, and that the frontier orbital energy gap is 2.12 eV. The lower the energy gap the more easily are the electrons excited from the ground to the excited state. By using the HOMO and LUMO energy values, the global chemical reactivity descriptors such as hardness, chemical potential, electro-negativity and electrophilicity index as well as local reactivity can be defined [51]. Pauling introduced the concept of electro-negativity as the power of an atom in a molecule to attract electrons to it. Hardness (η), chemical potential (μ) and electro-negativity (χ) are defined using Koopman's theorem as $\eta = (I\text{-}A)/2 = 1.06$, $\mu = -(I + A)/2 = -7.121$ and $\chi = (I + A)/2 = 7.121$, where A and I are the ionization potential and electron affinity of the molecule. $I = -E_{HOMO} = 8.181$ eV and $A = -E_{LUMO} = 6.061$ eV. One can also relate the stability of the molecule to hardness, which means that the molecule with a lower energy gap shows higher reactivity. Parr et al. [52] have defined a descriptor to quantify the global electrophilic power of the molecule as the electrophilicity index, $\omega = \mu^2/2\eta = 23.92$. The usefulness of this new reactivity quantity has been demonstrated recently in understanding the toxicity of various pollutants in terms of their reactivity and site selectivity [53].

Table 2
Calculated (scaled) wavenumbrs, observed IR, Raman bands and assignments.

B3LYP/6-31++G(d)(6D,7F)			IR	Raman	Assignments[a]
υ(cm^{-1})	IRI	RA	υ(cm^{-1})	υ(cm^{-1})	–
3103	3.16	262.12	–	–	υCHI(96)
3101	13.66	29.96	–	–	υCHI(87), υCH(12)
3092	4.57	23.94	–	–	υCHI(22), υCH(61)
3090	1.48	72.34	–	–	υCHI(97)
3081	11.20	70.62	3083	–	υCHI(61), υCHII(16), υCH(19)
3075	0.91	48.78	–	–	υCHII(63), υCH(21)
3071	25.26	114.71	–	–	υCHII(95)
3055	7.27	83.88	–	3057	υCHII(91)
3052	20.19	61.62	3053	–	υCHII(96)
3048	1.39	26.95	3035	–	υCH(91)
2993	36.01	92.40	–	–	υCH_3(92)
2991	22.26	32.24	–	–	υCH_3(96)
2987	94.58	332.00	–	–	υCH_3(95)
2981	0.06	13.72	2975	2972	υCH_3(99)
2925	49.27	390.00	2929	2930	υCH_3(99)
2921	30.13	8.94	–	–	υCH_3(100)
2912	18.02	78.12	2908	2910	υCH(95)
1656	157.58	64.27	1660	1659	υC═O(61), υC═C(18)
1599	45.61	89.80	1603	1600	υPhII(58), υPhI(23)
1580	657.43	3628.00	1578	–	υC═C(48), υPhI(12)
1572	99.16	3814.60	–	1568	υPhI(64), υPhII(10)
1548	11.59	312.92	–	–	υPhI(62), υPhII(11)
1544	66.66	566.26	–	1525	υPhII(57), υPhI(20)
1495	23.70	79.51	1488	–	δCHII(20), υPhII(52)
1471	15.81	93.09	–	–	δCHI(55), υPhI(26)
1470	7.61	2.77	–	–	δCH_3(74)
1465	11.78	21.34	1462	1459	δCH_3(88)
1454	3.59	3.82	–	–	δCH_3(88)
1451	0.02	12.62	–	–	δCH_3(90)
1407	34.74	59.16	1403	–	υPhII(44), δCHII(15), δCH(10)
1385	5.33	11.46	–	–	δCH_3(93)
1381	18.36	89.61	1382	–	υPhI(64), δCHI(21)
1365	5.00	0.21	1362	–	δCH_3(93)
1342	4.65	8.27	1344	–	δCH(48), δCHII(18), υPhII(17)
1321	186.18	48.03	1324	–	δCH(30), δCHII(13)
1312	9.03	351.29	–	1314	δCH(49), υCC(15)
1302	1.98	13.28	–	1300	δCH(77)
1289	5.74	15.02	1292	–	υPhI(88)
1279	98.22	123.56	1281	1282	υCC(13), δCHII(50), δCH(10)
1276	2.96	5.57	–	–	δCHI(65)
1272	2.57	116.07	–	–	υPhII(53)
1199	14.45	210.97	–	–	δCH(23), δPhII(19), υCC(40)
1193	64.81	25.52	–	–	δPhII(13), υCC(46), υPhII(13)
1186	159.77	40.27	1185	1185	υCC(47), δCH(11)
1171	16.29	536.14	1172	–	δCHII(59)
1162	84.96	31.59	1155	–	δCHI(65)
1136	5.06	13.78	–	–	δCH_3(44), υPhII(14)
1101	4.70	3.05	1105	–	δCHII(47), υPhII(25)
1094	9.92	4.26	1090	1092	δCHI(53), υPhI(30)
1082	0.73	12.04	–	–	υCC(50), δCH_3(28)
1064	119.04	80.25	1059	1058	υCCl(15), δCHI(55)
1040	15.11	28.03	–	1035	δCH_3(47), υPhII(15), δCH(12)
1010	129.28	253.74	1010	1010	υCC(47), υPhI(18)
994	4.49	4.19	–	–	δCHII(55), υPhII(11)
988	32.88	5.23	–	986	γCH(43), τC═C(24), δPhI(12)
986	128.42	39.08	984	986	δPhI(58)
957	0.30	2.39	954	–	γCHI(85)
943	0.19	0.80	–	–	γCHII(87)
936	1.52	0.61	–	–	γCHII(77), τPhII(16)
931	0.59	2.37	–	–	γCHI(62)
931	0.32	5.57	–	–	γCHI(11), δCH_3(52), υCC(10)
904	0.48	1.11	–	898	δCH_3(76), δCC(15)
873	6.67	21.34	875	874	δCC(10), γCH(43),

(*continued on next page*)

Table 2 (*continued*)

B3LYP/6-31++G(d)(6D,7F)			IR	Raman	Assignments[a]
υ(cm^{-1})	IRI	RA	υ(cm^{-1})	υ(cm^{-1})	–
					δC═C(12), δC═O(10)
866	1.83	12.60	–	–	υCC(66), δCH3(13)
858	0.39	14.19	–	–	γCH(49), γC═O(11)
828	3.37	3.36	830	–	γCHI(45), γCHII(27)
814	0.82	1.06	–	–	γCHII(90)
811	45.70	1.11	812	–	γCHI(24), γCHII(57)
801	41.64	0.88	–	–	γCHI(69)
790	26.17	16.21	788	–	δPhII(14), υCC(16), δPhI(10), υPhII(14)
73613.52	3.49	734	734	υPhII(40),	τPhI(10),
γC═O(10),	γCC(16)				
717	8.97	34.75	720	–	υPhI(49), υCCl(12)
706	0.49	7.42	–	–	τPhI(22), τPhII(20), υCCl(43)
671	11.65	2.35	669	–	υCC(19), δC═O(32) δPhI(12)
656	6.89	0.48	–	648	τPhI(33), γC═O(36)
629	1.39	19.86	632	626	δPhII(78)
618	2.42	4.50	–	–	δPhI(84)
550	6.25	6.57	–	555	δPhII(25), δCC(35), δC═C(10)
534	26.88	1.41	538	–	τPhII(33), τCC(39)
516	17.92	13.12	514	–	δCC(25), δC═O(12)
488	16.81	18.52	490	492	δCCl(18), δCC(28), δC═C(11)
465	9.33	0.16	466	-τPhI(42),	γCCl(30), γCC(16)
446	3.58	1.62	–	–	δCC(42), δPhII(11)
404	0.46	0.20	–	–	τPhI(27), τPhII(43)
401	0.36	0.37	–	–	τPhI(56), τPhII(25)
393	0.10	0.66	–	–	τPhII(50), γCC(12)
372	12.54	9.20	–	375	δCC(28), δPhI(10)
318	3.10	1.41	–	319	δCC(40), δCCl(17), δC═O(10)
304	0.90	0.70	–	–	δCC(24), δCCl(26)
270	0.24	3.31	–	–	γCC(18), γCCl(13)
257	0.52	0.23	–	–	τCH_3(38), δCC(12), τPhII(11)
251	0.94	2.19	–	–	τPhII(23), δCC(13), γCC(14)
241	1.27	0.85	–	–	τCH_3(38), δCCl(11), δCC(11)
218	0.83	0.15	–	–	τCH_3(77)
205	2.55	0.46	–	–	δCC(41), τCH_3(28)
162	0.32	2.06	–	158	δPhII(11), δCC(17)
143	0.32	1.79	–	–	δCC(27), τCC(22)
129	1.06	2.00	–	–	δCC(16), γCC(34)
102	0.16	3.35	–	98	τCC(24), τPhI(13), δCC(18), τC═C(13)
77	2.89	0.65	–	75	τCC(19), τPhI(17), τC═O(16), γCC(13)
55	0.14	1.38	–	–	τCC(33), τPhII(22)
41	0.01	2.86	–	–	δCC(12), γCC(10), τCC64
35	0.02	1.87	–	–	δC═C(22), δCC(37)
25	0.04	3.71	–	–	τC═O(58), δCC(14)
17	0.04	0.55	–	–	τCC(67)

δ-in-plane deformation; γ-out-of-plane deformation; τ-torsion; PhI-phenyl ring with clorine; PhII-phenyl ring with methyl; potential energy distribution (%) is given in brackets in the assignment column; IR_I-IR intensity; R_A-Raman activity.

[a] υ-stretching.

4.4. Nonlinear optical studies

Nonlinear optics deals with the interaction of applied electromagnetic fields in various materials to generate new electromagnetic fields, altered in wavenumber, phase, or other physical properties [54]. Quantum chemical calculations have been shown to be useful in the description of the relationship between the electronic structure of systems and its NLO response [55]. The computational approach allows the determination of molecular NLO properties as an inexpensive way to design molecules by analyzing their potential before synthesis and to determine high order hyperpolarizability tensors of the molecules. The first order hyperpolarizability of the title compound is calculated and is found to be 10.90×10^{-30} esu. The calculated hyperpolarizability of the title compound is 83.85 times that of the standard NLO material urea (0.13×10^{-30}esu) [56]. The theoretical second order hyperpolarizability was calculated using the Gaussian09 software and is equal to -30.35×10^{-37} e.s.u. We conclude that the title compound

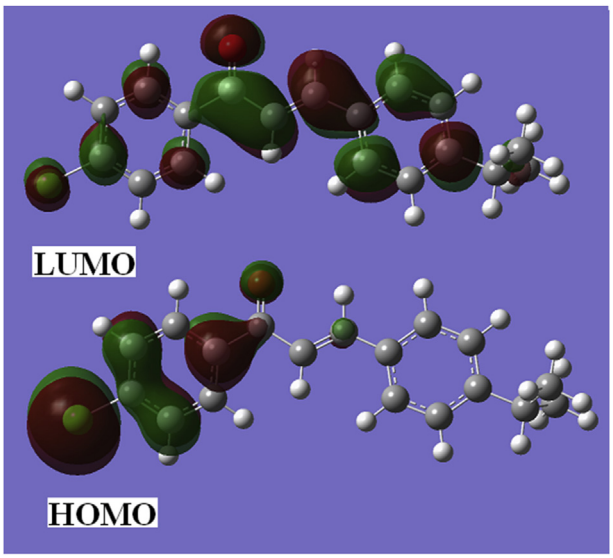

Fig. 4. HOMO, LUMO plots of (2*E*)-1-(4-chlorophenyl)-3-[4-(propan-2-yl)phenyl]prop-2-en-1-one.

and its derivatives are an attractive object for future studies of nonlinear optical properties.

4.5. Molecular electrostatic potential

Molecular electrostatic potential (MEP) at a point in space around a molecule gives information about the net electrostatic effect produced at that point by the total charge distribution over the molecule [57]. Moreover, the MEP surface helps to predict the reactivity of a wide variety of chemical systems in both electrophilic and nucleophilic reactions, the study of biological recognition processes and hydrogen bonding interactions [58]. It also provides visual understanding of the relative polarity of the molecule. The different values of the electrostatic potential at the surface are represented by different colors; red represents regions of most electro negative electrostatic potential, blue represents regions of most positive electrostatic potential and green represents regions of zero potential. The electrostatic potential increases in the order red < orange < yellow < green < blue [57]. To predict reactive sites for electrophilic and nucleophilic attack in the investigated molecule, the MEP surface is plotted for the title compound at DFT level [59]. Fig. 5 shows the electrostatic potential contour map of the title compound. The negative electrostatic potential corresponds to an attraction of a proton by the aggregate electron density in the molecule (shades of red and yellow) and the positive electrostatic potential corresponds to the repulsion of a proton by the nuclei (shades of blue). As can be seen from Fig. 5, the negative electrostatic potential regions are mainly localized over the carbonyl group, the phenyl rings and are possible sites for electrophilic attack. The positive regions are localized over all the hydrogen atoms as possible sites for nucleophilic attack.

4.6. Natural bond orbital analysis

The natural bond orbitals (NBO) calculations were performed using NBO 3.1 program [60] as implemented in the Gaussian09 package at the DFT/B3LYP level and the possible intensive interaction are given in Table 3.

The important inter-molecular hyper-conjugative interactions are: C_4–C_6 from Cl_1 of $n_1(Cl_1)\rightarrow\sigma^*(C_4–C_6)$, C_4–C_6 from Cl_1 of $n_2(Cl_1)\rightarrow\sigma^*(C_4–C_6)$, C_3–C_{28} from Cl_1 of $n_1(Cl_1)\rightarrow\sigma^*(C_3–C_{28})$, C_4–C_6 from O_2 of $n_1(O_2)\rightarrow\sigma^*(C_4–C_6)$ with electron densities, 0.01270, 0.01270, 0.06480, 0.01270 e and stabilization energies of 781.11, 423.83, 5426.1, 19.34 kJ/mol.

The NBO analysis also describes the bonding in terms of the natural hybrid orbital $n_3(Cl_1)$, which occupy a higher energy orbital (−0.42569 a.u.) with considerable p-character (100.00%) and low occupation number (1.92483) and $n_2(O_2)$, which occupy a higher energy orbital (−0.25981 a.u.) with considerable p-character (100.00%) and low occupation number (1.88747). The other orbitals are, $n_1(Cl_1)$ occupy a lower energy orbital(−0.93672 a.u.) with p-character (17.14%) and high occupation number (1.99293) and $n_1(O_2)$ occupy a lower energy orbital (−0.70170a.u.) with p-character (41.12%) and high occupation number (1.97827).

Thus, a very close to pure p-type lone pair orbital participates in the electron donation to the $n_1(Cl_1)\rightarrow\sigma^*(C_4–C_6)$, $n_2(Cl_1)\rightarrow\sigma^*(C_4–C_6)$, $n_1(Cl_1)\rightarrow\sigma^*(C_3–C_{28})$, $n_1(O_2)\rightarrow\sigma^*(C_4–C_6)$ interactions in the compound. The results are tabulated in Table 4.

4.7. Molecular docking studies

The lymphocyte-specific kinase (Lck) is a member of the Src family of non-receptor tyrosine kinases that plays an essential role for the selection and maturation of developing T-cell in the thymus and in mature T-cell function. Lck is considered an attractive cell-specific target for the design of novel T-cell immuno suppressants. Molecular docking simulations were performed on AutoDock-Vina software [61] and the 3D crystal structure of *Lck kinase* was obtained from Protein Data Bank (PDB ID: 1QPE) [62]. The protein was prepared for docking by removing the co-

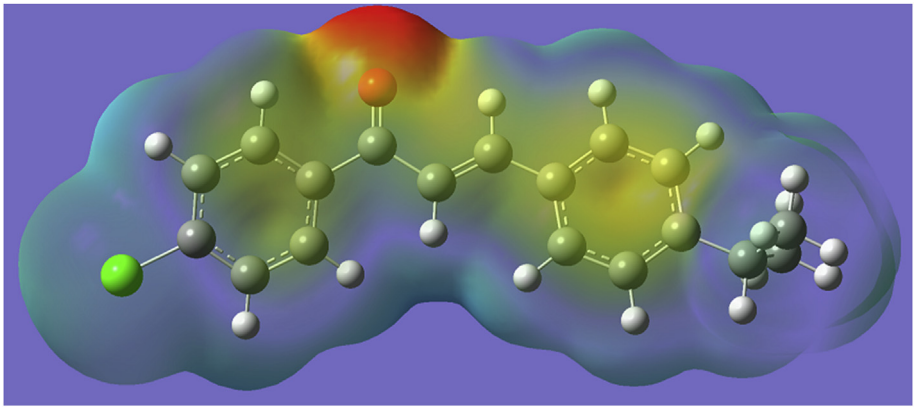

Fig. 5. MEP plot of (2*E*)-1-(4-chlorophenyl)-3-[4-(propan-2-yl)phenyl]prop-2-en-1-one.

Table 3
Second order perturbation theory analysis of Fock matrix in NBO basis corresponding to the Intra-molecular bonds of the title compound.

Donor(i)	Type	ED/e	Acceptor(j)	Type	Ed/e	E(2)[a]	E(j)-E(i)[b]	F(i,j)[c]
C3–C4	σ	1.98059	C4–C6	σ*	0.01270	79.08	0.47	0.173
_	–	–	C13–C18	σ*	0.02784	10.97	0.83	0.085
C3–C28	σ	1.97841	C3–C28	σ*	0.06480	4380.41	0.39	1.174
_	–	–	C4–C6	σ*	0.01270	728.79	1.32	0.876
_	–	C6–C8	σ*	0.02184	4199.40	0.40	1.153	
C4–C6	σ	1.98166	C3–C4	σ*	0.05666	1.75	1.19	0.041
_	–	–	C4–C6	σ*	0.01270	10.44	0.61	0.071
C6–C8	σ	1.97776	C4–C6	σ*	0.01270	19.26	0.57	0.094
_	–	–	C13–C18	σ*	0.02784	6.08	0.93	0.067
C13–C18	σ	1.97492	C9–C11	σ*	0.01273	2.26	1.04	0.043
_	–	–	C11–C13	σ*	0.02131	1.56	1.18	0.038
C31–C33	σ	1.98208	C4–C6	σ*	0.01270	15.80	0.61	0.088
_	–	–	C33–C34	σ*	0.02688	3.29	1.15	0.055
C33–C34	π	1.66857	C4–C6	σ*	0.01270	21.34	0.62	0.102
_	–	–	C31–C33	σ*	0.02737	2.87	1.27	0.054
LP Cl1	σ	1.99293	C4–C6	σ*	0.01270	2.16	0.81	0.037
_	–	–	C31–C33	σ*	0.02737	1.66	1.46	0.044
LP Cl1	π	1.97261	C4–C6	σ*	0.01270	423.83	0.36	0.350
_	–	–	C13–C18	σ*	0.02784	41.45	0.72	0.154
_	–	–	C33–C34	π*	0.38470	40.93	0.40	0.126
LP Cl1	n	1.92483	C3–C28	σ*	0.06480	5426.1	0.37	1.266
_	–	–	C4–C6	σ*	0.01270	781.11	1.30	0.913
_	–	–	C6–C8	σ*	0.02184	5342.80	0.38	1.288
LP O2	σ	1.97827	C3–C4	σ*	0.05666	1.66	1.15	0.039
_	–	–	C4–C6	σ*	0.01270	19.34	0.57	0.094

[a] E(2) means energy of hyper-conjugative interactions (stabilization energy in kJ/mol).
[b] Energy difference (a.u.) between donor and acceptor i and j NBO orbitals.
[c] F(i,j) is the Fock matrix elements (a.u.) between i and j NBO orbitals.

Table 4
NBO results showing the formation of Lewis and non-Lewis orbitals.

Bond(A-B)	ED/e[a]	EDA%	EDB%	NBO	s%	p%
σC3-C4	1.98059	48.88	51.12	$0.6992(sp^{1.81})C$	35.51	64.49
_	−0.59863	–	–	$+0.7150(sp^{2.14})C$	31.84	68.16
σC3-C28	1.97841	47.46	52.54	$0.6889(sp^{1.91})C$	34.34	65.66
_	−1.44360	–	–	$+0.7248(sp^{2.21})C$	31.15	68.85
σC4-C6	1.98166	50.31	49.69	$0.7093(sp^{1.64})C$	37.90	62.10
_	−0.73790	–	–	$+0.7049(sp^{1.66})C$	37.51	62.49
σC6-C8	1.97776	48.42	51.58	$0.6958(sp^{1.93})C$	34.13	65.87
_	−0.69572	–	–	$+0.7182(sp^{2.05})C$	32.73	67.27
σC13-C18	1.97492	50.58	49.42	$0.7112(sp^{2.10})C$	32.21	67.79
_	−0.62135	–	–	$+0.7030(sp^{2.82})C$	26.18	73.82
σC31-C33	1.98208	48.85	51.15	$0.6989(sp^{1.96})C$	33.74	66.26
_	−0.73450	–	–	$+0.7152(sp^{1.59})C$	38.59	61.41
πC33-C34	1.98191	51.43	48.57	$0.7172(sp^{1.00})C$	0.00	100.0
_	−0.74298	–	–	$+0.6969(sp^{1.00})C$	0.00	100.0
N1 Cl1	1.99293	–	–	$sp^{0.21}$	82.86	17.14
_	−0.93672	–	–	–	–	–
N2 Cl1	1.97261	–	–	$sp^{1.00}$	0.00	100.0
_	−0.48775	–	–	–	–	–
N3 Cl1	1.92483	–	–	$sp^{1.00}$	0.00	100.0
_	−0.42569	–	–	–	–	–
N1 O2	1.97827	–	–	$sp^{0.70}$	58.84	41.12
_	−0.70170	–	–	–	–	–
N2 O2	1.88747	–	–	$sp^{1.00}$	0.00	100.0
_	−0.25981	–	–	–	–	–

[a] ED/e is expressed in a.u.

crystallized ligands, water molecules and co-factors. AutoDockTools (ADT) graphical user interface was used to calculate Kollman charges and to add polar hydrogens. Ligand was prepared for docking by minimizing its energy at B3LYP/6-31++G(d)(6D, 7F) level of theory. Charges were calculated by Geistenger method. Active site of the protein was defined so as to include residues of the active site within the grid size of 40 Å × 40 Å × 40 Å. Docking protocol was tested by extracting co-crystallized inhibitor from the protein and then docking the same. Docking protocol which we employed predicted the same conformation as was present in the

crystal structure with RMSD value well within the reliable range of 2 Å. Amongst the docked conformations, one which binded at the active site with high affinity was visualized for detailed ligand-protein interactions in Discover Studio Visualizer 4.0 and Pymol software. The ligand binds at the catalytic site of substrate (Fig. 6) by weak non-covalent interactions most prominent of which are alkyl and alkyl-π interactions. TYR264, TYR304 and ARG302 hold the aromatic rings by alkyl- π interactions (Fig. 7). TYR304 forms a pi-pi stacking interaction with one of the phenyl rings. The inhibitor (2*E*)-1-(4-chlorophenyl)-3-[4-(propan-2-yl)phenyl]prop-2-en-1-one forms a stable complex with Lck. These preliminary results suggest that the compound might exhibit inhibitory activity against Lck. This may result in design of novel T-cell immunosuppressants. However biological tests need to be done so as to validate the computational predictions.

5. Conclusion

The vibrational spectroscopic studies of (2*E*)-1-(4-Chlorophenyl)-3-[4-(propan-2-yl)phenyl]prop-2-en-1-one were reported experimentally and theoretically. Potential energy distribution of normal modes of vibrations was done using GAR2PED program. MEP predicts the most reactive part in the molecule. The geometrical parameters obtained from theoretical calculations are in agreement with the XRD data.The calculated hyperpolarizability is high and the title compound and its derivatives are attractive object for future studies in nonlinear optics. For the title compound, HOMO is delocalized over the phenyl ring PhI and the carbonyl group while LUMO is delocalized over the entire molecule and this shows that an eventual charge transfer occurs within the molecule, and that the frontier orbital energy gap is 2.12 eV. The title compound binds at the catalytic site of substrate by weak non-covalent interactions most prominent of which are alkyl and alkyl-π interactions and forms a stable complex with Lck.

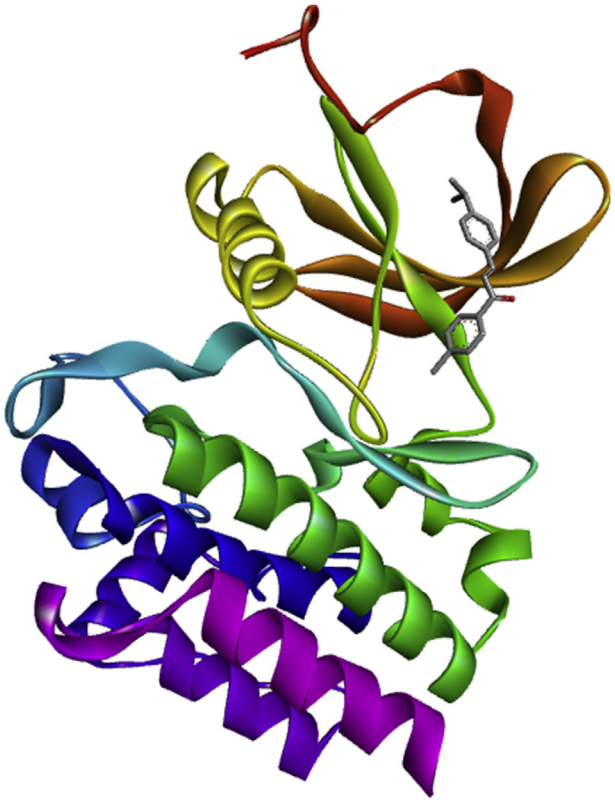

Fig. 6. The title compound, (2*E*)-1-(4-chlorophenyl)-3-[4-(propan-2-yl)phenyl]prop-2-en-1-one binds at the active site of Lck.

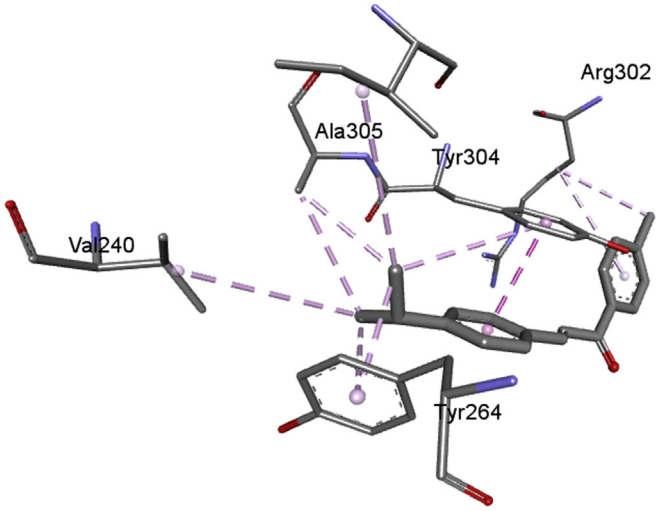

Fig. 7. Detailed interactions of (2*E*)-1-(4-chlorophenyl)-3-[4-(propan-2-yl)phenyl] prop-2-en-1-one with the inhibitor residues, dotted lines represent the interactions.

Acknowledgements

The authors would like to extend their sincere appreciation to the Deanship of Scientific Research at King Saud University for funding this work through the Research Group Project No. PRG-1436-23. BN thanks UGC for assistance through BSR and the authors are thankful to University of Antwerp for access to the university's CalcUA Supercomputer Cluster.

Appendix A. Supplementary data

Supplementary data related to this article can be found at http://dx.doi.org/10.1016/j.molstruc.2016.05.030.

References

[1] B.K. Sarojini, B. Narayana, B.V. Ashalatha, J. Indira, K.G. Lobo, J. Cryst. Growth 295 (2006) 54–59.
[2] S. Shettigar, G. Umesh, K. Chadrasekharan, B.K. Sarojini, B. Narayana, Opt. Mater. 30 (2008) 1297–1303.
[3] P. Poornesh, S. Shettigar, G. Umesh, K.B. Manjunatha, K.P. Kamath, B.K. Sarojini, B. Narayana, Opt. Mater. 31 (2009) 854–859.
[4] J. Indira, P.P. Karat, B.K. Sarojini, J. Cryst. Growth 242 (2002) 209–214.
[5] S.F. Nielsen, S.B. Christensen, G. Cruciani, A. Kharazmi, T. Liljefors, J. Med. Chem. 41 (1998) 4819–4832.
[6] C.W. Mai, M. Yaeghoobi, N. Abd-Rahman, Y.B. Kang, M.R. Pichika, Eur. J. Med. Chem. 77 (2014) 378–387.
[7] M. Wan, L. Xu, L. Hua, A. Li, S. Li, W. Lu, Y. Pang, C. Cao, X. Liu, P. Jiao, Bioorg. Chem. 54 (2014) 38–43.
[8] S. Mukherjee, V. Kumar, A.K. Prasad, H.G. Raj, M.E. Bracke, C.E. Olsen, S.C. Jain, V.S. Parmar, Bioorg. Med. Chem. 9 (2001) 337–345.
[9] Y.M. Lin, Y. Zhou, M.T. Flavin, L.M. Zhou, W. Nie, F.C. Chen, Bioorg. Med. Chem. 10 (2002) 2795–2802.
[10] S.N. Lopez, M.V. Castelli, S.A. Zacchino, J.N. Dominguez, G. Lobo, C.C. Jaime, J.C.G. Cortes, J.C. Ribas, C. Devia, M.R. Ana, D.E. Ricardo, Bioorg. Med. Chem. 9 (2001) 1999–2013.
[11] Z.N. Siddiqui, T.N.M. Musthafa, A. Ahmad, A.U. Khan, Bioorg. Med. Chem. Lett. 21 (2011) 2860–2865.
[12] A. Agarwal, K. Srivastava, S.K. Puri, P.M.S. Chauhan, Bioorg. Med. Chem. 13 (2005) 4645–4650.
[13] B. Insuasty, A. Montoya, D. Becerra, J. Quiroga, R. Abonia, S. Robledo, I.D. Velez, Y. Upegui, M. Nogueras, J. Cobo, Eur. J. Med. Chem. 67 (2013) 252–262.
[14] R. Abonia, D. Insausty, J. Castillo, B. Insausty, J. Quiroga, M. Nogueras, J. Cobo, Eur. J. Med. Chem. 57 (2012) 29–40.
[15] V. Sharma, A. Chaudhary, S. Arora, A.K. Saxena, M.P.S. Ishar, Eur. J. Med. Chem. 69 (2013) 310–315.

[16] S. Shenvi, K. Kumar, K.S. Hatti, K. Rijesh, L. Diwakar, Eur. J. Med. Chem. 62 (2013) 435–442.
[17] A.M. Asiri, M. Karabacak, S. Sakthivel, A.O. Al-youbi, S. Muthu, S.A. Hameed, S. Renuga, T. Alagesan, J. Mol. Struct. 1103 (2016) 145–155.
[18] S. Parveen, M.A. Al-Alshaikh, C.Y. Panicker, A.A. El-Emam, B. Narayana, V.V. Saliyan, B.K. Sarojini, C. Van Alsenoy, J. Mol. Struct. 1112 (2016) 136–146.
[19] I. Kulai, S. Mallet-Ladeira, J. Mol. Struct. 1104 (2016) 14–18.
[20] A. Abbas, H. Gokce, S. Bahceli, M. Bolte, M.M. Naseer, J. Mol. Struct. 1112 (2016) 124–135.
[21] S. Demir, F. Tinmazy, N. Dege, I.O. Ilhan, J. Mol. Struct. 1108 (2016) 637–648.
[22] J.P. Jasinski, R.J. Butcher, K. Veena, B. Narayana, H.S. Yathirajan, Acta Cryst. E65 (2009) o1965–o1966.
[23] J.P. Jasinski, C.J. Guild, S. Samshuddin, B. Narayana, H.S. Yathirajan, Acta Cryst. E66 (2010) o2018–o2018.
[24] J.P. Jasinski, J.A. Golen, P.S. Nayak, B. Narayana, H.S. Yathirajan, Acta Cryst. E68 (2012) o366–o366.
[25] R.J. Butcher, H.S. Yathirajan, H.G. Anilkumar, B.K. Sarojini, B. Narayana, Acta Cryst. E62 (2006) o1633–o1635.
[26] R.J. Butcher, H.S. Yathirajan, B.K. Sarojini, B. Narayana, A. Mithun, Acta Cryst. E62 (2006) o1629–o1630.
[27] R.J. Butcher, H.S. Yathirajan, H.G. Anilkumar, B.K. Sarojini, B. Narayana, Acta Cryst. E62 (2006) o1659–o1661.
[28] R.J. Buctcher, H.S. Yathirajan, B. Narayana, A. Mithun, B.K. Sarojini, Acta Cryst. E63 (2007) o30–o32.
[29] W.T.A. Horrison, H.S. Yathirajan, B.K. Sarojini, B. Narayana, K.K. Vijay Raj, Acta Cryst. E62 (2006) o1578–o1579.
[30] Y.S. Mary, K. Raju, C.Y. Panicker, A.A. Al-Saadi, T. Thiemann, C. Van Alsenoy, Spectrochim. Acta 128 (2014) 638–646.
[31] Y.S. Mary, K. Raju, C.Y. Panicker, A.A. Al-Saadi, T. Thiemann, Spectrochim. Acta 131 (2014) 471–483.
[32] F.M. Sun, J.S. Wang, T.W. Traxler, Chemosphere 40 (2000) 1417–1425.
[33] B. Narayana, V.V. Salian, B.K. Sarojini, J.P. Jasinski, Acta Cryst. E70 (2014) o855–o855.
[34] Gaussian 09, Revision C.01, M.J. Frisch, G.W. Trucks, H.B. Schlegel, G.E. Scuseria, M.A. Robb, J.R. Cheeseman, G. Scalmani, V. Barone, B. Mennucci, G.A. Petersson, H. Nakatsuji, M. Caricato, X. Li, H.P. Hratchian, A.F. Izmaylov, J. Bloino, G. Zheng, J.L. Sonnenberg, M. Hada, M. Ehara, K. Toyota, R. Fukuda, J. Hasegawa, M. Ishida, T. Nakajima, Y. Honda, O. Kitao, H. Nakai, T. Vreven, J.A. Montgomery Jr., J.E. Peralta, F. Ogliaro, M. Bearpark, J.J. Heyd, E. Brothers, K.N. Kudin, V.N. Staroverov, T. Keith, R. Kobayashi, J. Normand, K. Raghavachari, A. Rendell, J.C. Burant, S.S. Iyengar, J. Tomasi, M. Cossi, N. Rega, J.M. Millam, M. Klene, J.E. Knox, J.B. Cross, V. Bakken, C. Adamo, J. Jaramillo, R. Gomperts, R.E. Stratmann, O. Yazyev, A.J. Austin, R. Cammi, C. Pomelli, J.W. Ochterski, R.L. Martin, K. Morokuma, V.G. Zakrzewski, G.A. Voth, P. Salvador, J.J. Dannenberg, S. Dapprich, A.D. Daniels, O. Farkas, J.B. Foresman, J.V. Ortiz, J. Cioslowski, D.J. Fox, Gaussian, Inc., Wallingford CT, 2010.
[35] J.B. Foresman, in: E. Frisch (Ed.), Exploring Chemistry with Electronic Structure Methods, A Guide to Using Gaussian, Pittsburg, PA, 1996.
[36] R. Dennington, T. Keith, J. Millam, Gaussview, Version 5, Semichem. Inc., Shawnee Missions, KS, 2009.
[37] J.M.L. Martin, C. Van Alsenoy, GAR2PED, a Program to Obtain a Potential Energy Distribution from a Gaussian Archive Record, University of Antwerp, Belgium, 2007.
[38] N.P.G. Roeges, A Guide to the Complete Interpretation of IR Spectra of Organic Compounds, Wiley, New York, 1994.
[39] N.B. Colthup, L.H. Daly, S.E. Wiberly, Introduction to IR and Raman Spectroscopy, Academic Press, New York, 1990.
[40] R.M. Silverstein, F.X. Webster, Spectrometric Identification of Organic Compounds, sixth ed., John Wiley, Asia, 2003.
[41] G. Socrates, Infrared Characteristic Group Frequencies, John Wiley and Sons, NewYork, 1981.
[42] N. Sundaraganesan, C. Meganathan, B.D. Joshua, P. Mani, A. Jayaprakash, Spectrochim. Acta 71 (2008) 1134–1139.
[43] R. Renjith, Y.S. Mary, C.Y. Panicker, H.T. Varghese, M.P. Parys, C.V. Alsenoy, T.K. Manojkumar, Spectrochim. Acta 124 (2014) 480–491.
[44] W.O. George, P.S. Mcintyre, Infrared Spectroscopy, first ed., John Wiley and sons, Chichester, 1987.
[45] Y.S. Mary, K. Raju, I. Yildiz, O. Temiz-Arpaci, H.I.S. Nogueira, C.M. Granadeiro, C. Van Alsenoy, Spectrochim. Acta 96 (2012) 617–625.
[46] J. Coates, in: R.A. Meyers (Ed.), Interpretation of Infrared Spectra, a Practical Approach, John Wiley and Sons Inc, Chichester, 2000.
[47] G. Varsanyi, Assignments of Vibrational Spectra of Seven Hundred Benzene Derivatives, Wiley, New York, 1974.
[48] J.B. Bhagyasree, H.T. Varghese, C.Y. Panicker, J. Samuel, C. Van Alsenoy, K. Bolelli, I. Yildiz, E. Aki, Spectrochim. Acta 102 (2013) 99–113.
[49] Y.S. Mary, K. Raju, C.Y. Panicker, A.A. Al-Saadi, T. Thiemann, Spectrochim. Acta 131 (2014) 471–483.
[50] K. Fukui, Science 218 (1982) 474–754.
[51] R.G. Parr, P.K. Chattaraj, J. Am. Chem. Soc. 113 (1991) 1854–1855.
[52] R.G. Parr, L. Szentpaly, S. Liu, J. Am. Chem. Soc. 121 (1999) 1922–1924.
[53] R. Parthasarathi, J. Padmanabhan, V. Subramanian, B. Maiti, P. Chattaraj, Curr. Sci. 86 (2004) 535–542.
[54] Y.R. Shen, The Principles of Nonlinear Optics, Wiley, New York, 1984.
[55] D.M. Burland, R.D. Miller, C.A. Walsh, Chem. Rev. 94 (1994) 31–75.
[56] M. Adant, L. Dupuis, L. Bredas, Int. J. Quantum Chem. 56 (2004) 497–507.
[57] P. Thul, V.P. Gupta, V.J. Ram, P. Tandon, Spectrochim. Acta 75 (2010) 251–260.
[58] P. Politzer, J.S. Murray, in: D.L. Beveridge, R. Lavery (Eds.), Theoretical Biochemistry and Molecular Biophysics, a Comprehensive Survey, Protein, vol. 2, Adenine Press, Schenectady, New York, 1991.
[59] A.D. Becke, J. Chem. Phys.I 98 (1993) 5648–5682.
[60] E.D. Glendening, A.E. Reed, J.E. Carpenter, F. Weinhold, NBO Version 3.1, Theoretical Chemistry Institute and Department of Chemistry, University of Wisconsin, Madison, 1988.
[61] O. Trott, A.J. Olson, J. Comput. Chem. 31 (2010) 455–461.
[62] X. Zhu, J.L. Kim, J.R. Newcomb, P.E. Rose, D.R. Stover, L.M. Toledo, H. Zhao, K.A. Morgenstern, Struct. Fold. Des. 7 (1999) 651–661.